PHYSICAL REVIEW C VOLUME 23, NUMBER 5 MAY 1981

β-γ angular correlation in ^{20}Na

R. E. Tribble*
Department of Physics, Princeton University, Princeton, New Jersey 08540
and Department of Physics and Cyclotron Institute, Texas A&M University, College Station, Texas 77843

D. P. May and D. M. Tanner
Cyclotron Institute, Texas A&M University, College Station, Texas 77843
(Received 19 November 1980)

The β-γ angular correlation for the decay of ^{20}Na has been measured using a symmetric four detector system. The ^{20}Na activity was produced by the ^{20}Ne$(p,n)^{20}$Na reaction and transported by a He jet to the detector chamber. Care was exercised to ensure that the β source was well defined. Correlation data were acquired for $\theta_{\beta-\gamma}=90°$ and 180° as a function of positron energy. The correlation data were analyzed for both linear and quadratic energy dependence. We report as the best estimate for the linear coefficient $(-5.0\pm0.8)\times10^{-3}$ MeV^{-1} and for the quadratic coefficient $(2.9\pm0.8)\times10^{-4}$ MeV^{-2}. Incorporating the results with other measurements in the $A=20$ system, we find an upper limit for the second class current contribution to the correlation which is no more than 20% of the weak magnetism contribution and is consistent with zero.

[NUCLEAR REACTIONS Radioactivity ^{20}Na; measured β-γ angular correlation. Determined induced weak currents.]

I. INTRODUCTION

Recently,[1] we gave a detailed accounting of our measurement of the β-γ angular correlation for the decay of

$$^{20}\text{F}\to{}^{20}\text{Ne}^*\,(2^+,\,E_x=1.63\text{ MeV})+e^-+\bar{\nu}$$
$$\quad\hookrightarrow{}^{20}\text{Ne}+\gamma(E2).$$

Here we report the results of the β-γ angular correlation for the analog decay of ^{20}Na. As we pointed out in Ref. 1, the results of the angular correlations can be used to study recoil-order induced interactions; in particular, we are interested in the strength of the second class current (SCC) interaction in $A=20$.

We expect the experimental angular correlation to be of the form (see Ref. 1 and references quoted therein)

$$W_\pm(\theta_{\beta-\gamma})=1+p_\pm\cos^2\theta_{\beta-\gamma}\,, \tag{1}$$

with

$$p_\pm\simeq\frac{E}{4m_nAc}\left[1\pm b\mp d_{II}-d_I-\frac{3}{2\sqrt{14}}\,\frac{j_2}{m_nA}\,(E_0-2E)-\frac{3}{\sqrt{35}}\,\frac{j_3}{m_nA}E\right], \tag{2}$$

where the + (−) represents electron (positron) decay, $E(E_0)$ is the beta energy (endpoint energy), m_n is the nucleon mass, and A is the nuclear number. (The vector second forbidden contributions to $p_\pm$ are expected to be small and have been ignored.[1]) The lower case letters represent beta-decay form factors that are commonly known as Gamow-Teller (c), weak magnetism (b), first-class induced tensor (d_I), second-class induced tensor (d_{II}), and second forbidden axial vector (j_2 and j_3). The form factors can be related to single-particle nuclear matrix elements via the impulse approximation.[2] As examples, the Gamow-Teller (c) and weak magnetism (b) form factors have the well-known impulse approximation form

$$c=g_A\left\langle\beta\left|\left|\sum_i\tau_i\vec{\sigma}_i\right|\right|\alpha\right\rangle, \tag{3a}$$

$$b=A\left(g_v\left\langle\beta\left|\left|\sum_i\tau_i\vec{l}_i\right|\right|\alpha\right\rangle+g_m\left\langle\beta\left|\left|\sum_i\tau_i\vec{\sigma}_i\right|\right|\alpha\right\rangle\right), \tag{3b}$$

where $g_v=1$, $g_A=1.23$, and $g_m=4.7$ and is the difference between the neutron and proton magnetic moments.

The G-parity transformation property can be used to help separate the b and d_{II} form factors from d_I, j_2, and j_3. Combining the ^{20}F and ^{20}Na correlation yields

$$p(^{20}\text{F})-p(^{20}\text{Na})\simeq\frac{E}{2m_nAc}\left[b-d_{II}-\frac{3}{2\sqrt{14}}\,\frac{j_2}{m_nA}\,\Delta(E_0)\right], \tag{4}$$

where $\Delta(E_0)=E_0(^{20}\text{Na})-E_0(^{20}\text{F})=5.8$ MeV, and j_2 and j_3 are assumed to be purely first-class interactions. If we add the predictions for the two correlations, we find

$$p(^{20}\mathrm{F})+p(^{20}\mathrm{Na}) \simeq \frac{E}{2m_n Ac}\left[1-d_I+\frac{3}{\sqrt{14}}\frac{j_2 E}{m_n A}-\frac{3}{2\sqrt{14}}\frac{j_2}{m_n A}\Delta'(E_0)-\frac{3}{\sqrt{35}}\frac{j_3}{m_n A}E\right], \tag{5}$$

where $\Delta'(E_0)=E_0(^{20}\mathrm{Na})+E_0(^{20}\mathrm{F})=16.6$ MeV. By invoking the conserved vector current (CVC) hypothesis,[3] the weak magnetism form factor can be predicted from the isovector width of the $M1$ gamma decay between the analog state (2^+, $T=1$, $E_x=10.273$ MeV) and the first excited state (2^+, $T=0$, $E_x=1.634$ MeV) in ^{20}Ne. The result is

$$b=\left(\frac{6\Gamma_{m_1}M^2}{\alpha E_\gamma^{\,3}}\right)^{1/2}=42.7\pm1.2\,, \tag{6}$$

where Γ_{m_1} is the isovector $M1$ width,[4] M is the nuclear mass, $\alpha=\frac{1}{137}$, and E_γ is the γ transition energy. The form factor c can be determined from the beta decay ft value by the relation[2]

$$c^2=\frac{6165}{ft}\,. \tag{7}$$

Using the ^{20}F ft value,[5] we find that $c=0.256\pm0.006$. According to the impulse-approximation prediction, the ratio b/Ac is nearly independent of nuclear number. For the $A=20$ system, we find that $(b/Ac)_\gamma=8.34\pm0.30$ by invoking the CVC.

Experiments sensitive to recoil-order induced interactions have been carried out in $A=8$, 12, and 19, as well as $A=20$. While initial results in $A=12$ (Ref. 6) and $A=19$ (Ref. 7) suggested the need for a sizable SCC, the most recent results in all three systems, $A=8$,[8] $A=12$,[9] and $A=19$ (Ref. 10) are consistent with CVC and not SCC. In addition to our measurements in $A=20$, Dupuis-Rolin *et al.* have reported measurements of both ^{20}Na (Refs. 11 and 12) and ^{20}F (Ref. 12) β-γ angular correlations. Their experiments were carried out with a very different target preparation technique than is reported here. After discussing our experimental procedure in Sec. II and the data analysis in Sec. III, we present our results in Sec. IV and compare them with those of Dupuis-Rolin *et al.*

II. EXPERIMENTAL PROCEDURE

The experiment was performed with the Princeton University AVF cyclotron. ^{20}Na was produced by the $^{20}\mathrm{Ne}(p,n)^{20}\mathrm{Na}$ reaction at $E_p=22$ MeV in a gas cell that was filled with 1 atm of Ne (90%)-He (10%) gas mixture. The ^{20}Na activity was transported by the He-jet technique through a Teflon capillary 1.78 mm in diameter and ≈ 3 m long. The experimental geometry is shown in Fig. 1. The source was produced by depositing the ^{20}Na activity on 0.0064 mm aluminized Mylar catcher foils. The source size was defined by a double collimator system. The first collimator was 2.2 mm in diameter while the second was 3.2 mm in diameter. The collimators were separated by 5 mm and the second one was located 1.6 mm from the catcher foil. Five catcher foils were attached to a foil holder assembly (see Fig. 1) with a spacing of 72° between each foil holder. The assembly was connected through a stainless steel shaft to a stepping motor. Once per sec the stepping motor

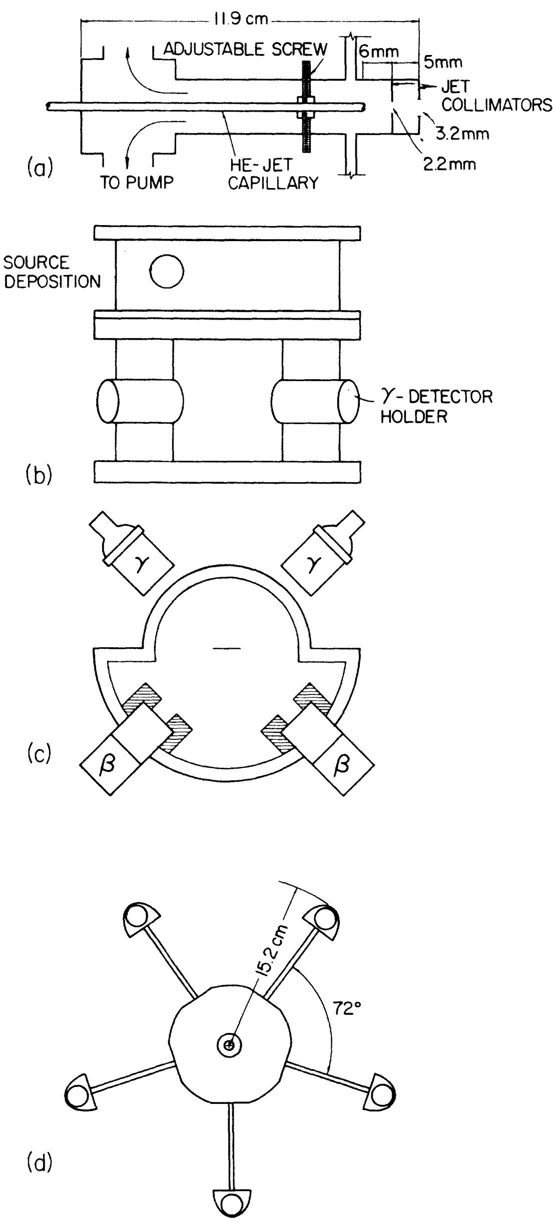

FIG. 1. (a) He-jet capillary holder and collimators; (b) side view, and (c) top view of the vacuum chamber; (d) target holder assembly.

rotated the foil holder assembly 144° (in ≈ 150 msec), thus transporting an activated foil into the counting region. By using five foils, background due to the long-lived positron emitters ^{11}C and ^{13}N was significantly reduced. During the foil rotation, the He-jet beam was interrupted by a chopper located between the two collimators.

A particularly troublesome feature of the He-jet technique is that β activity tends to migrate away from the catcher foil and deposits on chamber walls, etc. Much care was exercised in the present experimental design to mitigate this effect. First, the detector chamber was separated from the source production chamber, as shown in Fig. 1. The He jet was pumped by a 50-l/sec Roots pump[13] backed by a 24-l/sec two-stage rotary pump. A 250-l/sec turbomolecular pump was connected to the source production section of the apparatus and served to evacuate both the source and detector chamber. Lead inserts were used inside the production chamber to shield the detectors from the He jet and to limit the path available for activity to migrate into the detector region. In addition, stiff plastic "flaps" were inserted across the opening between the two chamber sections. As the target foils were rotated into the detector chamber, they passed through the flaps, which automatically closed to help block the migration of gas into the detector chamber. Under typical operating conditions, the vacuum at the capillary exit of the He jet was ≈250 μm at a gas flow rate of 1500 cm^3/min, while the production and detector chamber vacuum were maintained at < 1 μm.

The gas cell was set up on the 0° beam line at the Princeton University cyclotron facility. The He-jet capillary transported the activity through a 1 m thick concrete shielding wall to a quiet counting area. On-target beam currents averaged about 8 μA. At this intensity, the source strength averaged 10^6 disintegrations/sec during the part of the 1-sec cycle devoted to data acquisition. The detector chamber geometry was identical to that used for our ^{20}F measurement (Ref. 1). Two cylindrical plastic scintillators (7.62 cm diameter × 7.62 cm length) separated by 90° served as the β detectors, while two NaI detectors (7.62 cm diameter × 7.62 cm length) were used for γ detectors. The γ detectors could be moved to subtend relative β-γ angles between 90° and 180°. Under typical running conditions, the β and γ detectors were spaced 90° apart. Thus β-γ coincidence events for $\theta_{\beta-\gamma} = 90°$ and 180° could be recorded for each detector. A lead collimator was placed over the plastic scintillator so that positrons could enter the detector only through a 3.81 cm diameter circular aperture. The β and γ detectors encompassed 0.162 and 0.391 sr of solid angle, respectively.

Slow-fast electronics were used to record β-γ coincidences and energies. Data were routed to eight analog-to-digital converters (ADC's) and event-mode recorded on magnetic tape. The ADC signals corresponded to β energies (2 ADC's), γ energies (2 ADC's), and coincidence signals from time-to-amplitude converters (4 ADC's, one corresponding to each β-γ detector pair). Data acquisition and sorting analysis were performed with the acquisition code ACQUIRE.[14]

Two background tests were performed to check for activity depositing on the chamber walls or the catcher foil holders. Background data were recorded with the same electronics and coincidence requirements that were used for the experiment. With the stepping motor turned off, we observed a background rate of < 0.5% of the true event rate. In addition, the background was isotropic to < 10%, where the limit is strictly statistical. Thus this background rate would be a negligible contribution to the asymmetry (less than 0.05% for each datum point). To test for activity depositing on the catcher-foil holders, the foils were removed from the holder, and a stationary foil was mounted in line with the He jet with a geometry that closely simulated the actual catcher-foil geometry. With this setup, actuating the stepping motor did not produce a discernible increase in the background rate.

III. DATA ANALYSIS AND EXPERIMENTAL RESULTS

Data analysis followed much the same procedure as outlined in Ref. 1. Effects due to differences in γ-detector efficiencies were minimized by periodically reversing the position of the two detectors. Also, all of the final analysis used the ratio method for calculating the asymmetry. Denoting the two β detectors as 1 and 2, we calculated the asymmetry from the ratio

$$R = \left[\frac{N_1(180°)N_2(180°)}{N_1(90°)N_2(90°)} \right]^{1/2}, \tag{8}$$

where the angle denotes the β-γ coincidence angle.

Care was exercised in the analysis to check for energy dependent correlations between the β events and the time-of-flight (TOF) coincidence requirement. Two-dimensional spectra were generated to check the windows set on the TOF peaks to ensure that they would not induce energy-dependent asymmetries. Typical coincidence β and γ spectra are shown in Fig. 2. There is a significant background seen in the γ spectra that is due to coincidences between positrons and gammas from annihilation in flight. Gates were set on the γ

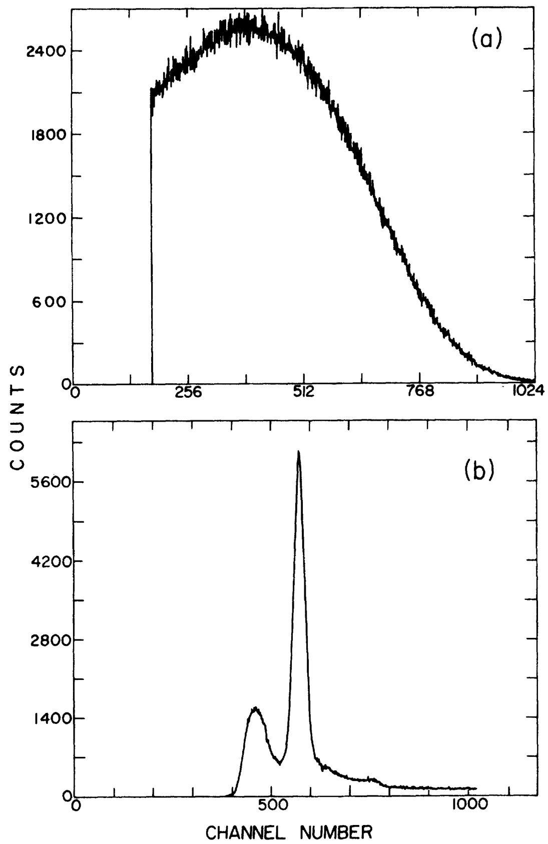

FIG. 2. Event spectra for (a) β's and (b) γ's in coincidence. In (b) a peak due to the addition of the 1.63 and 0.511 MeV γ peaks is discernible near channel 750. Also in (b) the Compton edge is just below a lower level discriminator.

spectra above the photopeak and the β-energy spectra were generated corresponding to these coincidence events. The ratio R was found to be nearly isotropic as a function of β energy for these data. A background subtraction was made on the "true" coincident data to account for the number of these events that fell within the window set on the photopeak. The error in this subtraction was assumed to be due to the statistical error in the background data. The final result for the ratio R contains this error estimate in quadrature with the statistical errors for each datum point.

The β-energy spectra were calibrated by calculating Kurie plots; a typical result is shown in Fig. 3. Only a limited region of the Kurie plot was used for the calibration to reduce distortions due to finite detector resolution, bremsstrahlung, and annihilation in flight. (The same detector and calibration techniques were used for the ^{20}F β-γ angular correlation reported in Ref. 1.) These effects are more serious for calibrating extremes of the β spectra. However, the statistics are poor for the high energy data and the background

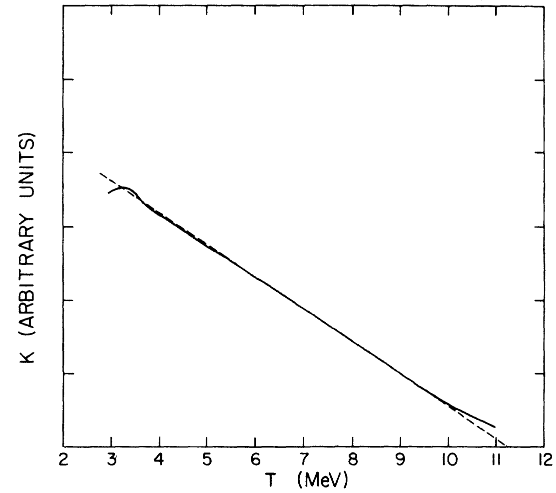

FIG. 3. Typical Kurie plot for a block of data. The solid line connects the data points and the dashed line is the detector calibration curve. The data points are separated by about 40 keV and the statistical uncertainty associated with each is on the order of the width of the line. The deviation of the Kurie plot at low positron energy is in the region where the background subtraction was significant.

precludes using the low energy data. The parameters obtained from the Kurie plots were checked over the course of the run to monitor small drifts in the β energies. The results for the ratio R as a function of β energy are shown in Fig. 4 and tabulated in Table I.

We have carried out several least squares fits to the data shown in Fig. 4. The ratio R can be

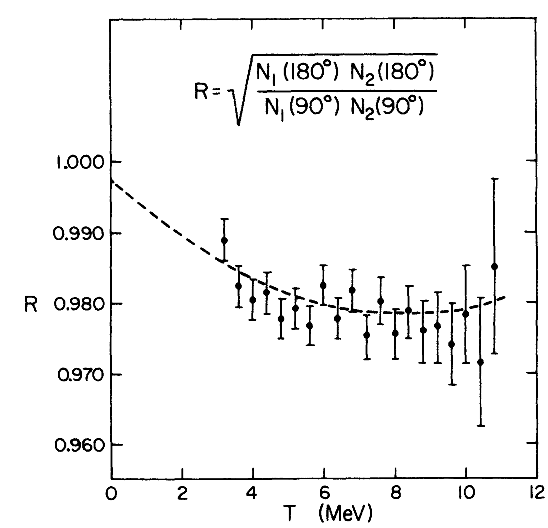

FIG. 4. Correlation data as a function of kinetic energy. The dashed line represents the second fit of Table II.

TABLE I. Results for the ratio R (see text) as a function of total positron energy.

E (MeV)	R
3.711	0.9889 ± 0.0030
4.111	0.9825 ± 0.0031
4.511	0.9805 ± 0.0030
4.911	0.9815 ± 0.0030
5.311	0.9778 ± 0.0029
5.711	0.9793 ± 0.0029
6.111	0.9767 ± 0.0029
6.511	0.9825 ± 0.0029
6.911	0.9778 ± 0.0029
7.311	0.9819 ± 0.0030
7.711	0.9752 ± 0.0031
8.111	0.9803 ± 0.0033
8.511	0.9756 ± 0.0036
8.911	0.9787 ± 0.0039
9.311	0.9759 ± 0.0044
9.711	0.9766 ± 0.0050
10.111	0.9740 ± 0.0059
10.511	0.9784 ± 0.0070
10.911	0.9716 ± 0.0093
11.311	0.9851 ± 0.0124

parametrized as

$$R = A + BE + CE^2 . \quad (9)$$

Results of the different least squares fits are given in Table II. When all three parameters (A, B, and C) are allowed to vary, the uncertainties in the B and C coefficients are expectedly quite large. We note that A is consistent with 1.0 in the three parameter fit. Since the experimental geometry for this correlation essentially was identical to that of the ^{20}F measurement (Ref. 1), the second least squares fit was obtained by adding the intercept determined from the linear least squares fit for our ^{20}F measurement as a datum point. This, in effect, ties down the intercept and significantly reduces the uncertainty in the B and C coefficients. The results quoted for the third least squares fit given in Table II were obtained by setting $A = 1.0$. As expected, this produces the lowest uncertainty for the B and C coefficients. Since the experimental geometry has been checked previously, the first least squares fit overestimates the uncertainty in B and C. The third fit, which assumes that the intercept is exactly 1.0, likely underestimates the uncertainty. Hence we adopt the results of the second fit as the best estimate of the B and C coefficients and their uncertainties.

All of the results quoted in Tables I and II have been corrected for the finite apertures in the β and γ detectors. As in Ref. 1, we have estimated the size of other possible energy dependent systematic effects such as positron annihilation in flight, bremsstrahlung, and source scattering. In all cases, these effects are significantly smaller than the uncertainties quoted for our results.

IV. DISCUSSION AND CONCLUSIONS

As we noted above, Dupuis-Rolin *et al.* recently reported[12] a result for the ^{20}F β-γ angular correlation, and in the same publication, they modified the ^{20}Na data of Ref. 11 to account for the finite geometry of their gas-cell β source. Their result for ^{20}F was in excellent agreement with our measurement of the ^{20}F correlation. Our result for the ^{20}Na correlation is in good agreement with the measurement quoted in Ref. 11, but after the corrections are made in Ref. 12, the agreement is only marginal. Quoting from Ref. 12, Dupuis-Rolin *et al.* find[15] $B = (-2.93 \pm 0.32) \times 10^{-3}$/MeV and $C = (0.78 \pm 0.40) \times 10^{-4}/\mathrm{MeV}^2$. The fit producing these results was performed by assuming that $A = 1.0$. This assumption likely underestimates the uncertainty in B and C. Clearly the best procedure for measuring the correlation coefficients is to allow A, B, and C to vary. However, as we noted above, this provides a very poor determination of both B and C. As a compromise, we choose to re-analyze the data of Ref. 12 and determine A from the ^{20}F data. (This is the same procedure that we used to obtain the second fit quoted in Table II.) Following this technique, the results of Ref. 12 for ^{20}Na becomes $B = (-2.9 \pm 0.8) \times 10^{-3}$/MeV and $C = (0.8 \pm 0.8) \times 10^{-4}/\mathrm{MeV}^2$.

TABLE II. Results for the least squares fits of the angular correlation data to a function $R = A + BE + CE^2$, where E is the total positron energy.

Fit	A	Coefficients B (10^{-3} MeV^{-1})	C (10^{-4} MeV^{-2})	χ_ν^2
three parameter	0.999 ± 0.010	−4.9 ± 2.9	2.8 ± 2.1	0.64
three parameter[a]	1.000 ± 0.0002	−5.0 ± 0.8	2.9 ± 0.8	0.60
two parameter		−5.0 ± 0.5	2.9 ± 0.6	0.60

[a] The intercept from the ^{20}F linear least squares fit of the angular correlation versus total electron energy was added as a datum point (1.000 ± 0.002 for $E = 0.0$).

We present first the predictions for the induced interactions from the β-γ angular correlations using only our results. With the B coefficient from the second least squares fit in Table II and the result for the ^{20}F correlation from Ref. 1, we find

$$\left(\frac{b-d_{II}}{Ac}\right)\simeq 10.5\pm 2.1\ , \qquad (10)$$

where the effect of the j_2 coefficient has been ignored. Removing the weak magnetism contribution, we find $d_{II}/Ac=-2.2\pm 2.1$. Including the effects of the second forbidden interactions, as in Ref. 1, we find the result $d_{II}/Ac=-2.6\pm 2.3$. By adding the correlations and correcting for second forbidden contributions, we find $d_I/Ac=6.8\pm 2.6$ where we assume a 100% uncertainty in the second forbidden correction (as in Ref. 1, we lower the uncorrected value of d_I/Ac by 1.6 with an uncertainty of 1.6).

Combining the modified results from Ref. 12 with those from our measurements, we find $B(^{20}\mathrm{F})=(0.5\pm 0.5)\times 10^{-3}/\mathrm{MeV}$, $B(^{20}\mathrm{Na})=(-4.0\pm 0.6)\times 10^{-3}/\mathrm{MeV}$, and $C(^{20}\mathrm{Na})=(1.8\pm 0.6)\times 10^{-4}/\mathrm{MeV}^2$. Once again we can extract a result for a second-class current by combining the two B coefficients to give

$$\left(\frac{b-d_{II}}{Ac}\right)=8.4\pm 0.8\ . \qquad (11)$$

Removing b/Ac via CVC, we find $d_{II}/Ac=-0.1\pm 0.9$. Including the possible second forbidden contributions, we find $d_{II}/Ac=-0.5\pm 1.1$. Adding the B coefficients from the combined experiments and correcting for second forbidden contributions, we find $d_I/Ac=5.0\pm 1.8$. The first class induced tensor interaction extracted from the combined data is consistent with the theoretical calculation of Calaprice *et al.*,[16] where they find $d_I/Ac=3.51$. The agreement is perhaps fortuitous, since meson exchange effects could significantly alter the impulse approximation prediction for the first-class induced tensor interaction. Also, the effect of the second forbidden contributions is not negligible in the extraction of the first-class tensor interaction.

From the above analysis, it is clear that a SCC is not required to explain the β-γ angular correlation results in $A=20$. These results would be more reliable if sufficient data were available to extract simultaneously the A, B, and C coefficients of Eq. (9). In order to achieve a reasonable level of uncertainty for d_{II}/Ac with a full three parameter fit, ten times more data for each correlation would be needed. With the present experimental configuration, this would require approximately twelve weeks of data acquisition for the ^{20}Na side of the correlation alone. While these measurements would be desirable, they do not seem to be critical at the present time. The results for the SCC interaction in $A=20$ are consistent with zero outside of the limits of the second forbidden corrections. Also, this system is in good agreement with recent measurements in $A=8$, 12, and 19 and suggests that SCC's may be absent. At most, they appear to be no more than 20% of the strength of weak magnetism.

ACKNOWLEDGMENTS

We would like to thank the staff at the Princeton University Cyclotron for their assistance. In particular, we would like to thank R. Kouzes and W. Moore, without whose help the experiment could not have been completed. We also acknowledge C. Jones and appreciate her assistance during the data analysis. This work was supported in part by the National Science Foundation, the Robert A. Welch Foundation, and the A. P. Sloan Foundation.

---

*Permanent address: Department of Physics and Cyclotron Institute, Texas A & M University, College Station, Texas 77843.

[1]R. E. Tribble and D. P. May, Phys. Rev. C 18, 2704 (1978).

[2]B. R. Holstein, Rev. Mod. Phys. 46, 789 (1974).

[3]M. Gell-Mann, Phys. Rev. 111, 362 (1958); R. P. Feynman and M. Gell-Mann, *ibid.* 109, 193 (1958).

[4]P. D. Ingalls, Nucl. Phys. A265, 93 (1976); L. K. Fifield, F. P. Calaprice, C. H. Zimmerman, M. J. Hurst, A. Pakkanen, T. G. M. Symons, F. Wett, and K. W. Allen, *ibid.* A288, 57 (1977).

[5]D. E. Alburger and F. P. Calaprice, Phys. Rev. C 12, 1690 (1975).

[6]K. Sugimoto, I. Tanihato, and J. Göring, Phys. Rev. Lett. 34, 1533 (1975).

[7]F. P. Calaprice, S. J. Freedman, W. C. Mead, and H. C. Vantine, Phys. Rev. Lett. 35, 1566 (1975).

[8]R. D. McKeown, G. T. Garvey, and C. A. Gagliardi, Phys. Rev. C 22, 738 (1980).

[9]P. Lebrun, Ph. Descheppor, L. Grenacs, J. Lehmann, C. Leroy, L. Palffy, A. Possoz, and A. Maio, Phys. Rev. Lett. 40, 302 (1978).

[10]W. E. Kleppinger, F. P. Calaprice, and D. Mueller, Bull. Am. Phys. Soc. 23, 603 (1978).

[11]N. Rolin, J. P. Deutsch, D. Favart, M. Lebrun, and R. Prieels, Phys. Lett. 70B, 23 (1977).

[12]N. Dupuis-Rolin, J. P. Deutsch, D. Favart, and R. Prieels, Phys. Lett. 79B, 359 (1978).

[13]Leybold-Heraeus model no. R-152.

[14]R. T. Kouzes, Nucl. Instrum. Methods 155, 261 (1978).

[15]Using the data from Ref. 12, we were not able to reproduce the uncertainties quoted in the reference for the ^{20}Na correlation coefficients. For the fit with $A = 1.0$, we find the uncertainties for B and C to be 0.5×10^{-3}/MeV and 0.6×10^{-4}/MeV, respectively.

[16]F. P. Calaprice, W. Chung, and B. H. Wildenthal, Phys. Rev. C 15, 2178 (1977).